The Astrophysical Journal, 853:22 (12pp), 2018 January 20 https://doi.org/10.3847/1538-4357/aa9ff1

Evolution and Photoevaporation of Protoplanetary Disks in Clusters: The Role of Pre-stellar Core Properties

Lin Xiao[1,2] and Qiang Chang[1]
[1] Xinjiang Astronomical Observatory, Chinese Academy of Sciences, 150 Science 1-Street, Urumqi 830011, People's Republic of China; xiaolin1702@126.com
[2] Key Laboratory for the Structure and Evolution of Celestial Objects, Chinese Academy of Sciences, Kunming 650011, People's Republic of China
Received 2017 June 22; revised 2017 December 3; accepted 2017 December 4; published 2018 January 18

Abstract

We explore the effects of progenitor pre-stellar core properties on the evolution of disks with external photoevaporation in clusters. Since the strength of external photoevaporation is largely determined by the depth of the gravitational potential well of the disk, the external photoevaporation rate is the function of star mass and disk size. The properties of a core collapse set up the initial conditions of protoplanetary disks, so they influence the evolutions of star mass and disk size. Our calculations show that the core properties can dramatically influence the efficiency of external photoevaporation. For the core with low angular velocity, most core mass directly falls onto the central star or onto the disk near the star. External photoevaporation is suppressed even if external radiation from nearby massive stars are strong. In this case, the disk evolution in clusters is primarily driven by its own internal viscosity. However, if the core angular velocity is high, most core mass falls onto the disk far from the central star. External photoevaporation is so strong that the disk mass is severely evaporated. Finally, the star mass is very low and the disk lifetime is very short. Our calculations could interpret some observational features of disks in clusters, such as the diameter distribution of disks in the Trapezium cluster and the correlation between mass accretion rate and star mass. We suggest that the disk mass determined by (sub)millimeter wavelength observations may be underestimated.

Key words: accretion, accretion disks – protoplanetary disks – stars: formation – stars: pre-main sequence

1. Introduction

The formation and evolution of protoplanetary disks around young stars in clusters are often influenced by the high stellar density or the ultraviolet radiation from nearby massive stars (e.g., Johnstone et al. 1998; Bonnell et al. 2003; Mitchell & Stewart 2010; Anderson et al. 2013; Kalyaan et al. 2015). Massive OB stars in clusters provide strong extreme-ultraviolet (EUV) and far-ultraviolet (FUV) radiation, and consequently the disks around the nearby low-mass stars may be heated and photoevaporated (e.g., O'dell et al. 1993; Henney & O'Dell 1999; Bally et al. 2000; Hatchell et al. 2013). The strong UV radiation from massive OB stars also produces bright ionization fronts from the outer part of protoplanetary disks (Vicente & Alves 2005). These features suggest that the properties of disks in clusters are different from those around isolated stars. For example, lifetimes of disks in clusters are much shorter due to high external photoevaporation rates (Da Rio et al. 2009; Reggiani et al. 2011). This makes giant planet formation by core accretion models difficult (e.g., Pollack et al. 1996; Hubickyj et al. 2005). Since most stars form in clusters (Lada & Lada 2003; Williams 2010; Mann et al. 2015), the properties of disks in these regions are crucial to understanding the diversity of extrasolar planets (e.g., Udry & Santos 2007; Howard 2013; Xie et al. 2016; Mills & Mazeh 2017).

Many surveys of protoplanetary disks in clusters have been performed to characterize the photoevaporation process and disk evolution (e.g., Carpenter 2002; Eisner & Carpenter 2003, 2006; Cieza et al. 2015; Mann et al. 2015). The Orion Nebula Cluster (ONC) is one of the ideal targets to investigate external photoevaporation (e.g., Mundy et al. 1995; Bally et al. 1998; Williams et al. 2005; Mann & Williams 2010; Eisner et al. 2016). Through centimeter wavelength Very Large Array observations, Churchwell et al. (1987) suggested that the mass-loss rate of the disk in ONC was very high ($\sim 10^{-7}$–$10^{-6}\ M_{\odot}\ \mathrm{yr}^{-1}$). Eisner et al. (2008) found the observational evidence of external photoevaporation of disks in ONC with the Combined Array for Research in Millimeter Astronomy and Submillimeter Array. Based on submillimeter absorption of protoplanetary disks, they found that disks in ONC were generally less massive than those in Taurus, and the most massive disks were rare near the ONC center, which suggested that photoevaporation might be dispersing disks. With the Atacama Large Millimeter/submillimeter Array (ALMA), Mann et al. (2014) further found that, at small separations (within 0.03 pc) from θ^1 Ori C, there was a clear drop in disk mass. Recently, the observations of seven protoplanetary disks near a B star in NGC 1997 by Kim et al. (2016) showed that even moderate FUV fluxes could drive high mass loss in the outer disk. Ansdell et al. (2017) confirmed the findings of Mann et al. (2014) and Kim et al. (2016) in the σ Orionis Cluster with ALMA. Champion et al. (2017) presented the observational results of four external photoevaporating disks in ONC through *Herschel* and ALMA surveys. Using a 1D disk model of the photodissociation region (e.g., Haworth et al. 2016), they reproduced the far-infrared line emission of the disk and proved that the disk dynamical evolution was driven by FUV photoevaporation with the mass-loss rates $\sim 10^{-7}$–$10^{-5}\ M_{\odot}\ \mathrm{yr}^{-1}$. Therefore, they predicted that these disks might have short lifetimes.

Theoretical studies of external photoevaporation in a protoplanetary disk are well established. Numerical simulations performed by Johnstone et al. (1998) and Adams et al. (2004) showed that external radiation fields due to nearby stars could drive significant disk mass loss. Since the external radiation flux is almost constant over the entire disk and the mass generally resides in the outer region of the disk, external photoevaporation can deplete the disk mass on short timescales. Adams et al. (2004) also derived analytic

approximations for the mass-loss rate due to external photoevaporation. Mitchell & Stewart (2010) suggested that the mass loss caused by external photoevaporation might transport disk mass from small radii to large, which could prevent the inward migration of Jupiter and Saturn and provided enough mass for the formation of Uranus and Neptune. Therefore, they considered that the solar system originated in clusters. Kalyaan et al. (2015) explored the structure of the disk with external photoevaporation and the non-uniform viscosity. They found that the surface density profile of the outer disk was very steep. Some studies also compare the theoretical predictions with the observations of protoplanetary disks in clusters (e.g., Clarke 2007; Anderson et al. 2013; Rosotti et al. 2017). Anderson et al. (2013) found that the external radiation was more efficient in the disk with large viscosity. They suggested that disks with large viscosities could expands outward easily. As a result, the disk size is very large. Since the gravitational potential is shallow at the large radii of the disk, the material in this region is easy to be evaporated by external radiations (Adams et al. 2004). The dependence of the external photoevaporation efficiency on the disk size is also found by Kalyaan et al. (2015). Anderson et al. (2013) also discussed that the star mass might influence the efficiency of external photoevaporation. Since the gravitational potential well is deeper for the massive star, it is difficult to evaporate the disk around it. Recently, Facchini et al. (2016) found that dust dragging and grain growth in the disk reduced the average cross-section at FUV wavelengths. They confirmed that external photoevaporation was very effective even in modest background field environments (e.g., Ansdell et al. 2016; Manara et al. 2016b, 2017; Pascucci et al. 2016; Alcalá et al. 2017; Mulders et al. 2017; Rafikov 2017). Their investigations imply that external photoevaporation may be the primary mechanism for determining the disk lifetime. Ndugu et al. (2017) performed the planet population synthesis in protoplanetary disks embedded in stellar clusters. They focused on the effect of background heating from nearby stars. The most important result is that the formation frequency of giant planets is low in cluster environments. Since the temperature of the outer disk is higher than the evaporation temperatures of some volatiles (e.g., CO), the amount of pebbles needed to form giant planets reduces and the formation timescales of giant planets exceed disk lifetimes.

Many studies show that the disk properties are not only determined by its own viscosity but also influenced by the initial conditions of the disk formation (e.g., Cassen & Moosman 1981; Vorobyov 2010; Xiao et al. 2017). According the standard star formation theory, protoplanetary disks form from the gravitational collapse of pre-stellar cores in molecular clouds (Shu 1977; McKee & Ostriker 2007). Core properties set up the initial conditions of disk formation (e.g., Cassen & Moosman 1981; Boss 1993; Kratter et al. 2010; Vorobyov 2010; Zhu et al. 2010). Bae et al. (2013) showed that the star mass and the disk size were determined by the angular velocity of the pre-stellar cloud core. For the case of the cloud core with high angular velocity, the initial angular momentum of the core is high. The materials with high angular momentum in the core fall onto the disk far from the central protostar (Hennebelle et al. 2004). The disk mass is large and easy to expand to large radius. As a result, the star mass is relatively low and the disk size is large. On the contrary, if the core angular velocity is low, then the star mass is high and the disk is small. Li & Xiao (2016) further investigated the influence of properties of pre-stellar cloud cores on disk lifetimes. They showed that the disk lifetime increased with the angular velocity of a cloud core. DeSouza & Basu (2017) found the relation between the disk accretion rate and the cloud core mass. They showed that the core mass influenced the strength of the gravitational torques of the disk and finally influenced the efficiency of accretion onto the star. Based on the studies of Li & Xiao (2016) and DeSouza & Basu (2017), Xiao et al. (2017) studied the evolutions of ice lines in disks with different core properties. If the angular velocity of the core is low, there is only one water ice line in the disk. However, if the angular velocity of the core is high, there are multiple ice lines in the disk.

Since the pre-stellar cloud core properties determine the disk properties and disk properties influence the effects of external photoevaporation, in this paper, we investigate the connection between the core properties and the external photoevaporation. We combine the long-term evolution disk model that includes mass infall from the pre-stellar cloud core (Xiao et al. 2017) with the existing external photoevaporation model (Anderson et al. 2013) to calculate disk masses, radii, and accretion rates. We attempt to understand how cloud core properties influence the efficiency of external photoevaporation. Finally, we investigate whether the combination of core properties with external photoevaporation can explain the observations of protoplanetary disks in clusters. This paper is organized as follows. In Section 2, we provide the details of our disk model, including cloud core properties, the basic equations, and photoevaporation rate from external FUV sources. Calculation results of the influence of core properties on external photoevaporation are presented in Section 3. We then discuss the implications of our calculation results for the observations in Section 4. Finally, conclusions are presented in Section 5.

2. Physical Model of Protoplanetary Disks

2.1. Initial Conditions for Disk Formation

Observations have revealed that young stellar objects are usually surrounded by disks with masses of about 0.001–0.1 $M_{\odot}$ (e.g., Beckwith et al. 1990; Hartmann et al. 1998; Andrews & Williams 2005, 2007; Andrews et al. 2009; Williams & Cieza 2011; Ansdell et al. 2016, 2017; Miotello et al. 2017). These disks are the byproducts of star formation, which originates from the collapse of a pre-stellar cloud core (e.g., Shu et al. 1987; McKee & Ostriker 2007). Goodman et al. (1993) suggested that most of the cloud cores rotated almost rigidly and slowly with an angular velocity on the order of $\sim 10^{-14}\,\mathrm{s}^{-1}$. In order to conserve angular momentum, protostar+disk systems must be formed. The disk obtains material from the infalling envelop of the core. Therefore, the properties of cloud cores set up the initial conditions of disk formation. Theoretical studies show that a pre-stellar cloud core can be treated as an isothermal sphere (Bonnor–Ebert sphere; Ebert 1955; Bonnor 1956). Shu (1977) predicted that the collapse of a cloud core was inside-out with a mass infall rate

$$\dot{M}_{\rm cd} = 0.975\frac{a^3}{G}, \quad (1)$$

where G is the gravitational constant and a is the isothermal sound speed. The timescale of the core collapse is estimated as

$$t_{\rm inf} = \frac{M_{\rm cd}}{\dot{M}_{\rm cd}}, \tag{2}$$

where $M_{\rm cd}$ is the mass of the pre-stellar cloud core. Following Cassen & Moosman (1981), Nakamoto & Nakagawa (1994) derived the mass influx, $S(R, t)$, onto the disk surface as a function of cylindrical radius, R, of the disk and time, t,

$$S(R, t) = \begin{cases} \dfrac{\dot{M}_{\rm cd}}{4\pi R R_{\rm d}(t)}\left[1 - \dfrac{R}{R_{\rm d}(t)}\right]^{-1/2} & \text{if } \frac{R}{R_{\rm d}(t)} < 1; \\ 0 & \text{otherwise,} \end{cases} \tag{3}$$

where $R_{\rm d}(t)$ is the centrifugal radius, which represents the maximum radius of the mass influx onto the disk:

$$R_{\rm d}(t) = \frac{1}{16} a\omega^2 t^3 = 31\left(\frac{\omega}{10^{-14}\ {\rm s}^{-1}}\right)^2\left(\frac{T_{\rm cd}}{10\ {\rm K}}\right)^{1/2} \times \left(\frac{t}{5 \times 10^5\ {\rm year}}\right)^3 {\rm au}, \tag{4}$$

where ω and $T_{\rm cd}$ are the angular velocity and temperature of a cloud core, respectively. After the core collapse ends, $R_{\rm d}(t)$ reaches the maximum value and $S(R, t)$ is set to 0. Notice that $R_{\rm d}(t)$ is proportional to ω^2 and $T_{\rm cd}^{1/2}$, which clearly indicates that the properties of pre-stellar cloud cores can influence the initial disk size. Equation (3) shows that for a fixed R, $S(R, t)$ decreases with $R_{\rm d}(t)$ increasing. It means that more materials fall onto the disk from the pre-stellar core. Therefore, during the core collapse, the disk mass is larger for the core with high ω. In the meantime, the protostar mass is lower. Since the external photoevaporation is the function of star mass and disk size (see Section 2.3), the efficiency of external photoevaporation should be different in disks with different core properties.

2.2. Disk Evolution Equations

In order to simulate the disk evolution from birth to death, the standard α-disk model is adopted (e.g., Nakamoto & Nakagawa 1994; Clarke et al. 2001; Armitage et al. 2003; Jin & Sui 2010; Anderson et al. 2013; Rafikov 2015; Rosotti et al. 2017). An accretion disk is an efficient machine for transporting material inward and angular momentum outward (e.g., Lynden-Bell & Pringle 1974; Pringle 1981; Cassen 1994). It is generally believed that the transport mechanism is the turbulence, although we have not yet understood the precise nature of the turbulence (e.g., Shakura & Sunyaev 1973; Hueso & Guillot 2005). Shakura & Sunyaev (1973) estimated that the typical size of the largest turbulent eddies could not exceed the disk thickness and the turnover velocity was subsonic. So, the effective turbulent viscosity, ν, is expressed as $\nu = \alpha c_{\rm s} h$, where $c_{\rm s}$ is the sound speed, h is the half thickness of the disk, and $\alpha \lesssim 1$ is a dimensionless parameter reflecting the viscosity strength. The basic equations, that describe the evolution of the disk surface density, Σ, are derived from the principles of fluid mechanics (Pringle 1981)

$$\frac{\partial \Sigma(R, t)}{\partial t} = \frac{3}{R}\frac{\partial}{\partial R}\left[R^{1/2}\frac{\partial}{\partial R}(\Sigma\nu R^{1/2})\right] + S(R, t) + S(R, t)\left\{2 - 3\left[\frac{R}{R_{\rm d}(t)}\right]^{1/2} + \frac{R/R_{\rm d}(t)}{1 + [R/R_{\rm d}(t)]^{1/2}}\right\} - \dot{\Sigma}_{\rm w}(R), \tag{5}$$

where $\dot{\Sigma}_{\rm w}(R)$ is the photoevaporation term. The diffusion equation described above is first derived by Jin & Sui (2010) and then improved by Xiao et al. (2017). During the core collapse, the protostar mass is usually lower than the disk mass. Therefore, the disk tends to be gravitationally unstable (e.g., Laughlin & Bodenheimer 1994; Vorobyov & Basu 2006; Machida et al. 2010). Spiral arms develop in the disk to redistribute mass and remove angular momentum (Kratter & Lodato 2016). After the collapse ending, the disk becomes gravitationally stable. The most promising mechanism driving turbulence may be the magnetorotational instability (MRI; Balbus & Hawley 1991). Since protoplanetary disks are cold and partially ionized, non-ideal magnetohydrodynamic (MHD) effects cannot be neglected (e.g., Gammie 1996; Fleming & Stone 2003; Bai & Stone 2011; Bai 2014; Lesur et al. 2014; Gressel et al. 2015).

Based on the above discussion, α is non-uniform in the disk and is a function of t:

$$\alpha = \max\left[\alpha_{\rm GI} + \alpha_{\rm MRI}, \alpha_{\rm min}\right], \tag{6}$$

where $\alpha_{\rm GI}$ is the viscosity parameter due to gravitational instability (GI; Laughlin & Bodenheimer 1994; Laughlin & Rozyczka 1996; Laughlin et al. 1997, 1998), $\alpha_{\rm MRI}$ is the viscosity parameter of MRI (Balbus & Hawley 1991, 1998), and $\alpha_{\rm min}$ is the minimum value for driving the disk evolution. Kratter et al. (2008) consider that $\alpha_{\rm GI} = (\alpha_{\rm short}^2 + \alpha_{\rm long}^2)^{1/2}$, where $\alpha_{\rm short} = \max\left[0.14(1.3^2/Q^2 - 1)(1 - u)^{1.15}, 0\right]$, $\alpha_{\rm long} = \max\left[1.4 \times 10^{-3}(2 - Q)/(u^{1.25}Q^{0.5}), 0\right]$, Q is the Toomre parameter (Toomre 1964), and u is the ratio of the disk mass to the mass of protostar+disk. We set $\alpha_{\rm MRI}$ according to the numerical results of Fleming & Stone (2003), who consider the non-ideal magnetohydrodynamic (MHD) effects in their 3D layered disk models. In the inner region of the disk, the temperature is so high that MRI can survive due to thermal ionization. We estimate the thermal ionization degree from the results of Umebayashi (1983). In the outer region, the disk is tenuous. Cosmic rays can penetrate the disk, thus the ionization is also high enough that the MRI can survive (Jin 1996). In the region where GI and MRI cannot survive, the hydrodynamic effects may drive the disk evolution. The viscosity caused by the hydrodynamics is still uncertain (e.g., Armitage 2011). We consider that $\alpha_{\rm min}$ is taken to be a constant, $\alpha_{\rm min} = 5 \times 10^{-4}$, which is the mean value of Dubrulle (1993), Klahr & Bodenheimer (2003), and Chambers (2006).

The disk temperature is calculated by the method of Nakamoto & Nakagawa (1994). They suggested that the energy flowed along the z-direction because the disk was geometrically thin. They further assumed that the energy generated locally in the disk was released by the thermal

radiation from the disk surface. The heating sources include viscous dissipation, irradiation from the protostar (Zhu et al. 2012), shock heating of the infalling material from mass influx onto the disk (Jin & Sui 2010), and thermal radiation from the ambient molecular cloud gas (Ciesla & Cuzzi 2006). Using the radiative diffusion approximation, they also derived the relation between the midplane temperature and the surface temperature for both optically thick and optically thin cases

$$\sigma T_s^4 = \frac{1}{2}\left(1 + \frac{1}{2\tau_p}\right)(\dot{E}_v + \dot{E}_s) + \sigma T_{\rm ir}^4 + \sigma T_{\rm cd}^4 \quad (7)$$

and

$$\sigma T_m^4 = \frac{1}{2}\left[\left(\frac{3}{8}\tau_R + \frac{1}{2\tau_p}\right)\dot{E}_v + \left(1 + \frac{1}{2\tau_p}\right)\dot{E}_s\right] + \sigma T_{\rm ir}^4 + \sigma T_{\rm cd}^4, \quad (8)$$

where T_s is the disk surface temperature, T_m is the disk midplane temperature, σ is the Stefan–Boltzmann constant, $\tau_p = \kappa_p\Sigma$ is the Planck mean optical depth, κ_p is the Planck mean opacity, $\dot{E}_v$ is the viscous dissipation rate, $\dot{E}_s$ is the energy generation rate by shock heating, and $T_{\rm ir}$ is the effective temperature of the irradiation suffered by the disk (Hueso & Guillot 2005), $\tau_R = \kappa_R\Sigma$ is the Rosseland mean optical depth, and κ_R is the Rosseland mean opacity, where $\kappa_p = 2.39\kappa_R$ (Nakamoto & Nakagawa 1994; Bell et al. 1997) for simplicity. The details of calculating parameters presented above can be seen in Jin & Sui (2010).

2.3. Photoevaporation

In this paper, we consider that photoevaporation of protoplanetary disks in clusters is due to radiation from both the host star and external stars. Although the host star generates EUV, FUV, and X-ray radiation, studies have shown that X-ray photoevaporation can produce a much higher mass-loss rate due to its ability to penetrate (e.g., Ercolano et al. 2009; Owen et al. 2010, 2011, 2012). Using radiation-hydrodynamic models, Owen et al. (2011, 2012) estimated the total mass-loss rate due to X-ray photoevaporation as follows:

$$\dot{M}_{\rm X} = 6.25 \times 10^{-9}\left(\frac{M_*}{1\ M_\odot}\right)^{-0.068} \times \left(\frac{L_{\rm X}}{10^{30}\ {\rm erg\ s^{-1}}}\right)^{1.14} M_\odot\ {\rm yr^{-1}}, \quad (9)$$

where M_* is the central star mass and $L_{\rm X}$ is the X-ray luminosity. According to Bae et al. (2013), $L_{\rm X}$ is a function of M_* for low-mass star ($M_* \leqslant 2\ M_\odot$):

$$\log(L_{\rm X}[{\rm erg\ s^{-1}}]) = 30.37(\pm 0.06) + 1.44(\pm 0.10) \times \log(M_*/M_\odot). \quad (10)$$

Owen et al. (2012) showed that the photoevaporation term of internal X-ray $\dot{\Sigma}_{\rm X}(R) = A\dot{\Sigma}_{\rm X,scale}$ and $\dot{\Sigma}_{\rm X,scale}$ was presented in their Appendix B. The scale coefficient, A, is determined by

$$\dot{M}_{\rm X} = A\int 2\pi R\dot{\Sigma}_{\rm X,scale}dR. \quad (11)$$

We use the same method adopted by Anderson et al. (2013) to calculate the photoevaporation term of external photoevaporation, $\dot{\Sigma}_{\rm F}(R)$. The basic model originates from Adams et al. (2004), who derived the semi-analytic expressions for the total mass-loss rate due to external FUV photoevaporation as a function of disk radius

$$\dot{M}_{\rm F} = Cn_d\langle\mu\rangle a_s R_g (R_g R)^{1/2} e^{-R_g/2R}, \quad (12)$$

where C is of the order of unity, n_d is the gas particle density at the disk edge, $\langle\mu\rangle$ is the mean particle mass (Adams et al. 2004), a_s is the sound speed at the sonic radius, and R_g is the gravitational radius, defined as (Anderson et al. 2013)

$$R_g = \frac{GM_*}{a_s^2} = \frac{GM_*\langle\mu\rangle}{kT_{\rm FUV}}\ {\rm au}, \quad (13)$$

where k is the gas constant and $T_{\rm FUV}$ is the function of the FUV flux G_0, estimated as follows (Kalyaan et al. 2015):

$$T_{\rm FUV} = 250\left(\frac{G_0}{3000}\right)^{1/2}\ {\rm K}. \quad (14)$$

The equations of external FUV photoevaporation discussed above show that the efficiency of external FUV photoevaporation is affected by the star mass and the disk size. If the star mass is low, the gravitational potential well is shallow. the mass-loss rate is high. The large disk size means that the gravitational potential well is shallow in the outer region of the disk. So external FUV photoevaporation is also effective. By assuming conservation of mass loss, Anderson et al. (2013) derived the relation of the photoevaporation term of external FUV, $\dot{\Sigma}_{\rm F}(R)$, as

$$\frac{d\dot{M}_{\rm F}}{dR} = 2\pi R\dot{\Sigma}_{\rm F}(R). \quad (15)$$

Finally, they solved the the FUV photoevaporation term

$$\dot{\Sigma}_{\rm F}(R) = \frac{B}{4\pi}\left(\frac{R_g}{R}\right)^{3/2}\left[1 + \frac{R_g}{R}\right]e^{-R_g/2R}, \quad (16)$$

where the parameter $B = Cn_d\langle\mu\rangle a_s$, which is estimated by fitting Equation (12) to the numerical results shown in Figure 4 of Adams et al. (2004). Anderson et al. (2013) considered that Equation (16) could well represent the physics of external FUV photoevaporation. We adopt the same expression as that used in Anderson et al. (2013), that $\dot{\Sigma}_{\rm w}(R) = \dot{\Sigma}_{\rm X}(R) + \dot{\Sigma}_{\rm F}(R)$. Although the photoevaporation of a disk in clusters comes from the combined effects of external FUV and internal X-ray radiations, external FUV radiation is the dominant dissipation mechanism for disks with low-mass stars. According to Equation (10), $L_{\rm X} \lesssim 10^{30}$ erg s^{-1} for the low-mass star ($M_* < 1\ M_\odot$). Figure 13 presented in Anderson et al. (2013) shows that when $L_{\rm X} \lesssim 10^{30}$ erg s^{-1}, the effect of the internal X-ray photoevaporation on the disk radius and mass is negligible.

3. Results

We start our models when the pre-stellar cloud core collapses. As discussed in the previous section, the properties of a cloud core are described by ω, $T_{\rm cd}$, and $M_{\rm cd}$. We focus on the disk formation around low-mass stars, so we set $M_{\rm cd} = 1.0\ M_\odot$ in this section. The typical value of $T_{\rm cd}$ is about 10 K (Goodman et al. 1993; Jijina et al. 1999; Caselli

et al. 2002). The average flux of the external FUV radiation is assumed to be $G_0 = 3000$ Habings, where Habings $= 1.6 \times 10^{-3}$ erg cm^{-2} s^{-1} (Habing 1968). The disk is assumed to be axisymmetric and radially divided into 300 logarithmically spaced points, with the inner and outer boundaries at $R_{\rm in} = 0.3$ au and $R_{\rm out} = 50{,}000$ au, respectively. We adopt a zero-torque condition at $R_{\rm in}$ and insure that the disk expands freely (Bath & Pringle 1981; Ruden & Lin 1986). We employ an explicit finite-difference integration scheme to solve Equation (5). The evolutions of disk mass, $M_{\rm disk}$, disk size, $R_{\rm disk}$, and mass accretion rate onto the protostar, $\dot{M}_{\rm acc}$, are also investigated. We adopt the same method introduced by Anderson et al. (2013) to determine $M_{\rm disk}$ and $R_{\rm disk}$. To calculate $\dot{M}_{\rm acc}$, We first determine the radial mass accretion rate within the disk, $\dot{M}$, according to Jin & Sui (2010):

$$\dot{M} = -6\pi R^{1/2}\frac{\partial}{\partial R}(\Sigma\nu R^{1/2}) + 4\pi R^2 S(R, t) \times \left[\left(\frac{R}{R_{\rm d}}\right)^{1/2} - 1\right], \quad (17)$$

and the steady-state accretion rate after the collapse ending is

$$\dot{M} = 3\pi\nu\Sigma\left[\left(\frac{R_*}{R}\right)^{1/2} - 1\right]^{-1}, \quad (18)$$

where R^* is the radius of the central star. We assume that $\dot{M}_{\rm acc}$ can be expressed as $\dot{M}_{\rm acc} = -\dot{M}(R_{\rm in})$. Then the growth rate of M_* is determined by

$$\dot{M}_*(t) = \int_0^{R_{\rm in}} 2\pi R S(R, t) dR + \dot{M}_{\rm acc}. \quad (19)$$

According to Equation (19), we derive $M_*(t)$ with setting $M_*(t = 0) \equiv 0$. Finally, we discuss the influence of core properties on the evolution of the external photoevaporating disk.

3.1. Disk Evolution Due to Internal X-Ray and External FUV Fields

We first assess the effects of external FUV photoevaporation by comparing the disk evolutions with and without external FUV fields. As shown in Figure 10 of Anderson et al. (2013), X-ray photoevaporation operates in the inner region of the disk (near the central star), while external FUV is effective in the outer region. This difference is very important to understand the disk evolutions with different photoevaporation mechanisms. Figure 1 shows the evolution of Σ of the internal X-ray photoevaporating disk with $\omega = 1.0 \times 10^{-14}$ s^{-1}, $T_{\rm cd} = 10$ K, and $M_{\rm cd} = 1.0\,M_\odot$. According to Equation (2), the timescale of the core collapse, $t_{\rm inf}$, is about 6.37×10^5 years. Before mass infall ending, shown in Figure 1(a), the mass supply from the collapsing cloud core is larger than the mass loss due to accretion and photoevaporation. Therefore, Σ increases and the disk expands. After mass infall ending, shown in Figure 1(b), the disk continues to expand due to its own internal viscosity (X-ray photoevaporation is weak in the outer region of the disk), and Σ decreases. As Σ decreases further, mass loss by internal X-ray photoevaporation in the inner region of the disk exceeds the mass supply by viscous accretion, so a gap forms near the star. After that, the disk dissipates inside out. The disk lifetime shown in Figure 1 is about 1.10×10^7 years.

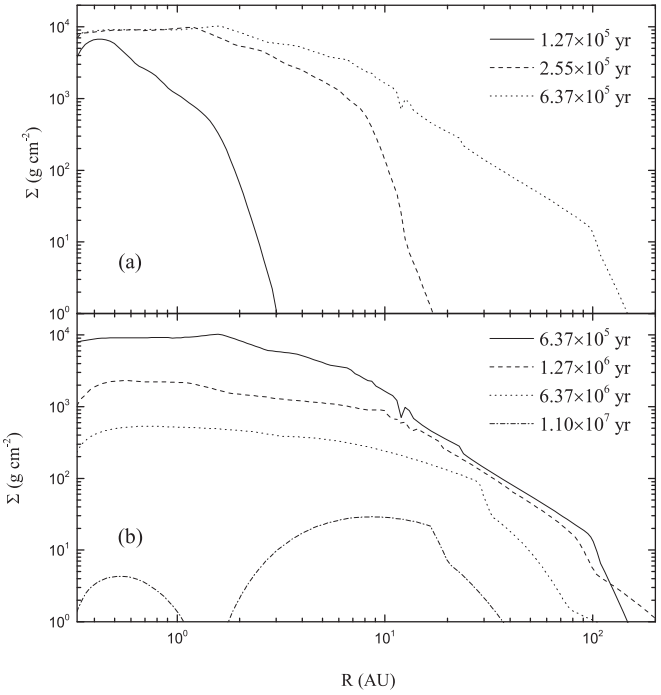

Figure 1. Evolution of Σ for the disk, including internal X-ray photoevaporation only, with $\omega = 1.0 \times 10^{-14}$ s^{-1}, $T_{\rm cd} = 10$ K, and $M_{\rm cd} = 1.0\,M_\odot$. The collapse timescale of the pre-stellar core is about 6.37×10^5 years. The top panel represents the evolution of Σ before core collapse stops. The bottom panel represents the evolution of Σ after core collapse stops. See the text for details.

We then add the effects of external FUV photoevaporation in the disk, and the evolution of Σ is shown in Figure 2. During the pre-stellar core collapse (Figure 2(a)), most of the material in the envelop falls onto the disk close to the central star and then is accreted onto the star. Therefore, in this stage the star grows fast and R_g is much larger than the disk size, $R_{\rm disk}$ (shown in Figure 4). External FUV photoevaporation is not effective (e.g., Adams et al. 2004). The mass loss due to external photoevaporation cannot offset the mass supply due to core collapse. The disk expands outward, but $R_{\rm disk}$ is smaller compared with that shown in Figure 1(a). After mass infall ends (Figure 2(b)), the disk tends to expand continuously due to the internal viscosity. In this stage, the mass supply stops, thus the external FUV photoevaporation becomes important. The main effects are that the outer disk is truncated and the overall surface density decreases. The disk has more sharp edge and dissipates from the outside in. Its lifetime (5.33×10^6 years) is half of that shown in Figure 1.

In Figure 3, we show $M_{\rm disk}$ and M_* as a function of t for the disk evolutions ($\omega = 1.0 \times 10^{-14}$ s^{-1}, $T_{\rm cd} = 10$ K, and $M_{\rm cd} = 1.0\,M_\odot$) with and without external FUV fields. During the core collapse, $M_{\rm disk}$ and M_* increase with t. Because there are more materials falling onto the disk than accreting and photoevaporating. The relatively low ω means that the central star gets a large amount of material from the pre-stellar core (Xiao et al. 2016). When the collapse ends, M_* is about $0.65\,M_\odot$, which is massive enough that the gravitational potential well is deep and external FUV photoevaporation is ineffective as discussed in the previous paragraph. The growths of $M_{\rm disk}$ and M_* are the same for cases with and without external photoevaporation. After the mass infall ending, external FUV photoevaporation becomes important. As a

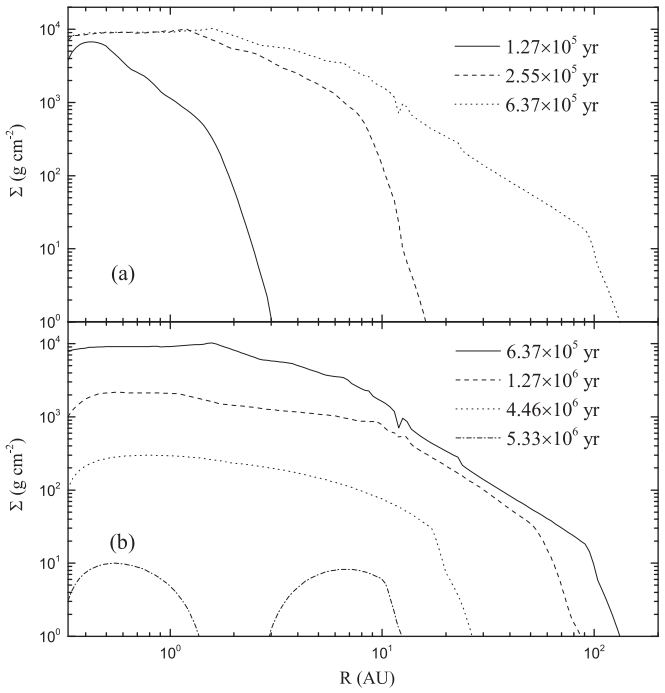

Figure 2. Evolution of Σ for the disk, including both internal X-ray and external FUV photoevaporations, with $\omega = 1.0 \times 10^{-14}$ s^{-1}, $T_{cd} = 10$ K, $M_{cd} = 1.0\ M_\odot$, and $G_0 = 3000$ Habings. The collapse timescale of the pre-stellar core is about 6.37×10^5 years. The top panel represents the evolution of Σ before core collapse stops. The bottom panel represents the evolution of Σ after core collapse stops. The disk lifetime is about half of that shown in Figure 1. See the text for details.

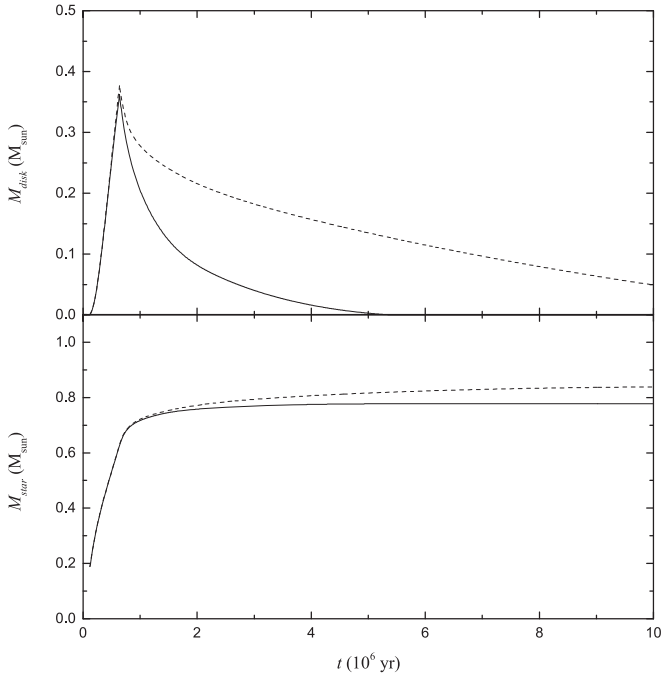

Figure 3. Evolution of M_{disk} (top panel) and M_* (bottom panel) as functions of t for the same core properties as those shown in Figures 1 and 2. Solid lines represent the case for including both internal X-ray and external FUV photoevaporations. Dashed lines represent the case for including internal X-ray photoevaporation only.

result, M_{disk} with external FUV photoevaporation decreases from 0.35 $M_\odot$ to 0 $M_\odot$ within 4.6×10^6 years. Since the effect of external photoevaporation is weak, the difference between the final star masses shown in Figure 3 is small ($\sim$0.05 $M_\odot$).

Figure 4 shows the disk size, R_{disk}, as a function of time, t, for the disk evolutions ($\omega = 1.0 \times 10^{-14}$ s^{-1}, $T_{cd} = 10$ K, and $M_{cd} = 1.0\ M_\odot$) with and without external FUV fields. Before the core collapse ends, M_* grows quickly, as shown in Figure 3. Therefore, R_g increases to 200 au within 2×10^5 years and $R_g \gg R_{disk}$. External photoevaporation is negligible (Adams et al. 2004). The growth of R_{disk} for disks with and without external FUV fields is identical: R_{disk} increases due to the mass supply from the collapsing core and the disk viscosity. When the core collapse is close to the end, the central star gets most of its final mass ($\sim$0.78 $M_\odot$, see Figure 3). So, the growth rate of R_g decreases and R_{disk} reaches $\sim$140 au, which is close to R_g. External photoevaporation becomes important, which causes R_{disk} to be smaller in the disk with external FUV fields. After the core collapse ends, mass supply to the disk stops. Since X-ray photoevaporation is weak in the outer region, the disk without external FUV fields expands due to its own internal viscosity all the time. Finally, R_{disk} for the disk without external FUV fields becomes larger than 10^4 au. However, external FUV photoevaporation is effective in the outer region of the disk. For the disk suffering external FUV photoevaporation, R_{disk} shrinks from 140 to 0 au within 4.6×10^6 years under the action of external photoevaporation, although it becomes more and more weak. This behavior, predicted by numerical models, is consistent with suggestions from disk observations (e.g., Eisner et al. 2008).

We compare $\dot{M}_{acc}$ as a function of t for the disk evolutions ($\omega = 1.0 \times 10^{-14}$ s^{-1}, $T_{cd} = 10$ K, and $M_{cd} = 1.0\ M_\odot$) with and without external FUV fields in Figure 5. The mass accretion

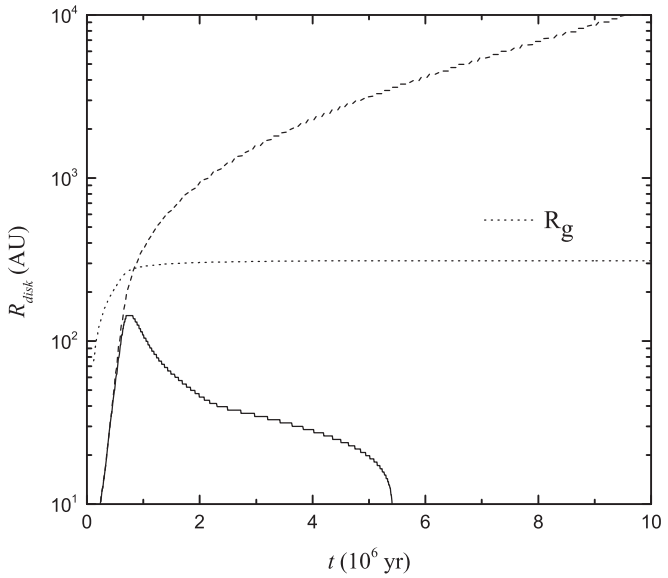

Figure 4. Evolution of R_{disk} and R_g as a function of t for the same core properties as those shown in Figures 1 and 2. The solid line represents the evolution of R_{disk} in the disk, including both internal X-ray and external FUV photoevaporations. The dashed line represents the evolution of R_{disk} in the disk, including internal X-ray photoevaporation only. The dotted line represents the evolution of R_g in the disk, including both internal X-ray and external FUV photoevaporations.

rate, $\dot{M}_{acc}$, is also the function of Σ near the star (Jin & Sui 2010). During the pre-stellar cloud core collapsing, the external FUV photoevaporation is weak, as discussed above. The evolutions of Σ are similar, as shown in Figures 1 and 2. Therefore, $\dot{M}_{acc}$ are identical in the early evolution of disks with

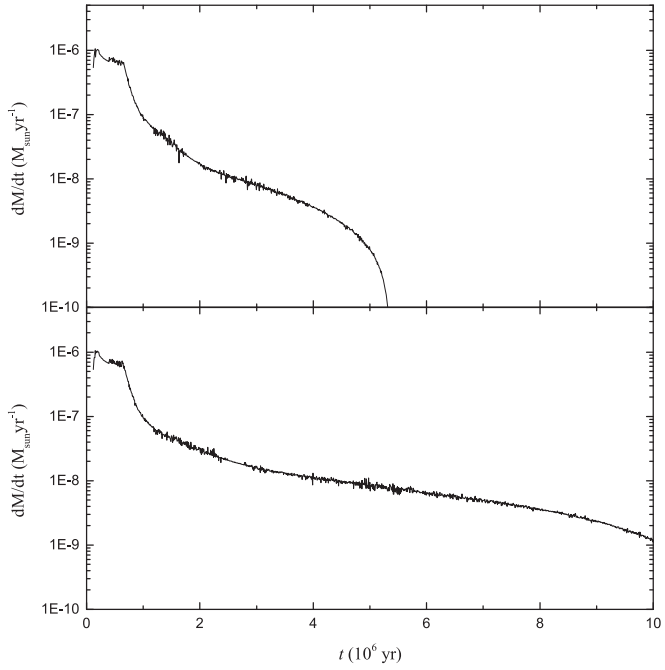

Figure 5. Evolution of $\dot{M}_{\rm acc}$ as a function of t for the same core properties as those shown in Figures 1 and 2. The top panel represents the case for including both internal X-ray and external FUV photoevaporations. The bottom panel represents the case for including internal X-ray photoevaporation only.

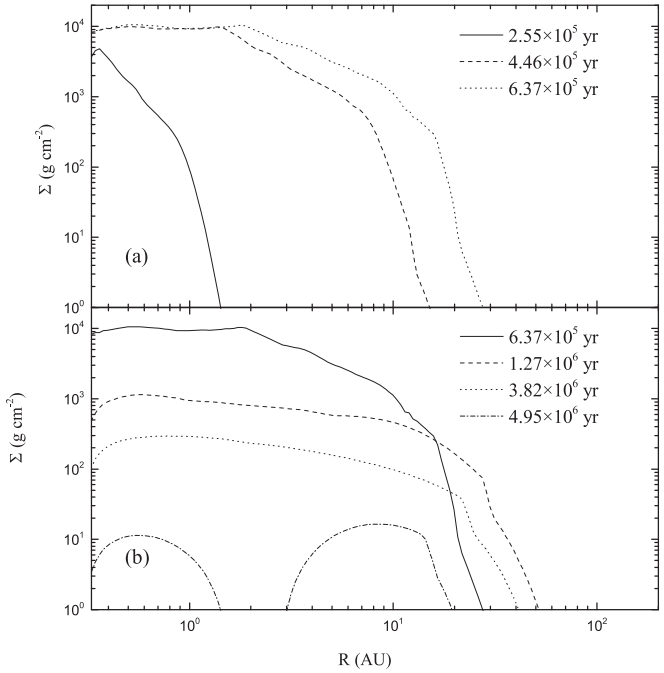

Figure 6. Evolution of Σ for the disk, including internal X-ray photoevaporation only, with $\omega = 0.3 \times 10^{-14}\,{\rm s}^{-1}$, $T_{\rm cd} = 10$ K, and $M_{\rm cd} = 1.0\ M_\odot$. The collapse timescale of the pre-stellar core is about 6.37×10^5 years. The top panel represents the evolution of Σ before core collapse stops. The bottom panel represents the evolution of Σ after core collapse stops. The disk lifetime is shorter than that shown in Figure 1. See the text for details.

and without external FUV fields. In this stage, $\dot{M}_{\rm acc}$ is very high ($\sim 10^{-7}$–$10^{-6}\,M_\odot\ {\rm yr}^{-1}$). After the core collapse ends, external FUV photoevaporation becomes important, as discussed in previous paragraphs. So, Σ in the disk with external photoevaporation decreases faster than that without external photoevaporation, which causes $\dot{M}_{\rm acc}$ to decrease more rapidly in the external FUV photoevaporating disk.

3.2. Evolution of External FUV Photoevaporating Disks with Different ω

In order to clarify the effects of ω on the efficiency of external FUV photoevaporation, we also present the results of the disk evolution, including internal X-ray photoevaporation, only with different ω. Observations of pre-stellar cloud cores suggest that the range of ω is about $\sim$0.1–13 $\times\ 10^{-14}\,{\rm s}^{-1}$ (e.g., Goodman et al. 1993; Jijina et al. 1999; Caselli et al. 2002). Our calculations indicate that when $\omega < 0.3 \times 10^{-14}\,{\rm s}^{-1}$, the angular momentum of the core is so low that it collapses onto the central star directly and no disk forms. We also notice that when $\omega > 5.0 \times 10^{-14}\,{\rm s}^{-1}$, the external FUV photoevaporation is so powerful that the material falling onto the disk from the core is evaporated immediately.

Figure 6 shows the evolution of Σ of the internal X-ray photoevaporating disk for the very low ω case that $\omega = 0.3 \times 10^{-14}\,{\rm s}^{-1}$, $T_{\rm cd} = 10$ K, and $M_{\rm cd} = 1.0\ M_\odot$. The evolutionary trend of Σ is similar to the typical case shown in Figure 1. Before core collapse ending, Σ increases and then decreases after that. The main difference is that the disk lifetime for $\omega = 0.3 \times 10^{-14}\,{\rm s}^{-1}$ is shorter ($\sim 4.95 \times 10^6$ years). Because the core mass falling onto the disk is less and most of it is close to the star. The material in the disk is accreted effectively onto the star. We then add the effect of external FUV photoevaporation in the disk with $\omega = 0.3 \times 10^{-14}\,{\rm s}^{-1}$, $T_{\rm cd} = 10$ K, and $M_{\rm cd} = 1.0\ M_\odot$. The evolution of Σ is shown in Figure 7. The trend of the disk evolution is similar to that with $\omega = 1.0 \times 10^{-14}\,{\rm s}^{-1}$ shown in Figure 2. Since most mass of the envelop during the core collapse falls directly onto the central star or onto the disk near the star for the low ω case, M_* grows quickly. The gravitational potential well (Equation (13)) is deeper in Figure 7 than that shown in Figure 2, which leads to the ineffective external FUV photoevaporation in the disk for the low ω case. Therefore, the difference in the disk lifetimes shown in Figure 7 and Figure 6 is small ($\sim 6.37 \times 10^5$ years), which indicates that the disk evolution with low ω in clusters is primarily driven by its own internal viscosity and internal X-ray photoevaporation.

In Figure 8, we show $M_{\rm disk}$ and M_* as functions of t for the disk evolutions ($\omega = 0.3 \times 10^{-14}\,{\rm s}^{-1}$, $T_{\rm cd} = 10$ K, and $M_{\rm cd} = 1.0\ M_\odot$) with and without external FUV fields. The evolutions of $M_{\rm disk}$ and M_* are similar to those shown in Figure 3. Since ω is smaller, more material of the core falls onto the star, which causes the star to grow faster and the disk to grow relatively slower. When the collapse ends, M_* is about 0.86 $M_\odot$ and $M_{\rm disk}$ is about 0.14 $M_\odot$. Therefore, the gravitational potential well is deeper, which results in the weaker external FUV photoevaporation. Finally, the difference between the final star masses shown in Figure 8 is smaller ($<0.002\ M_\odot$).

Figure 9 shows $R_{\rm disk}$ as a function of t for the disk evolutions ($\omega = 0.3 \times 10^{-14}\,{\rm s}^{-1}$, $T_{\rm cd} = 10$ K, and $M_{\rm cd} = 1.0\ M_\odot$). The evolutions of $R_{\rm disk}$ are similar to those shown in Figure 4. However, the lower ω means that the location of core mass falling onto the disk is closer to the star. So, $R_{\rm disk}$ for the disk without external FUV fields shown in Figure 9 is smaller than that shown in Figure 4. As discussed in previous paragraphs, the star gets more mass during the core collapse for the case of $\omega = 0.3 \times 10^{-14}\,{\rm s}^{-1}$. Therefore, R_g of the disk with external

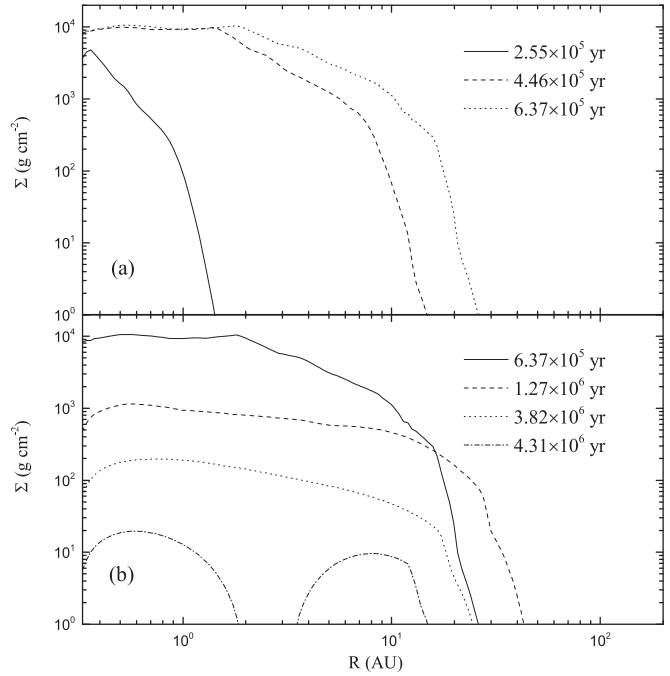

Figure 7. Evolution of Σ for the disk, including both internal X-ray and external FUV photoevaporations, with $\omega = 0.3 \times 10^{-14}\,s^{-1}$, $T_{cd} = 10$ K, $M_{cd} = 1.0\ M_{\odot}$, and $G_0 = 3000$ Habings. The collapse timescale of the pre-stellar core is about 6.37×10^5 years. The top panel represents the evolution of Σ before core collapse stops. The bottom panel represents the evolution of Σ after core collapse stops. The disk lifetime is close to that shown in Figure 6. See the text for details.

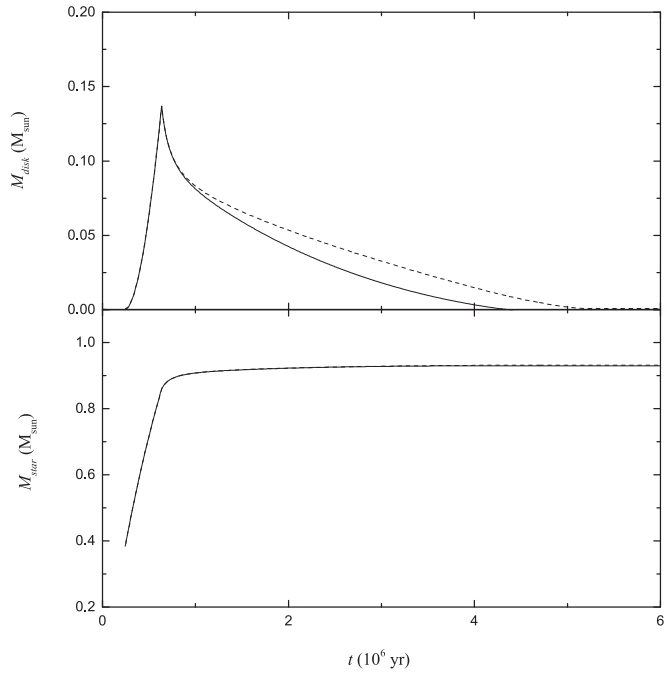

Figure 8. Evolution of M_{disk} (top panel) and M_* (bottom panel) as functions of t for the same core properties as those shown in Figures 6 and 7. The solid lines represent the case for including both internal X-ray and external FUV photoevaporations. The dashed lines represent the case for including internal X-ray photoevaporation only.

FUV photoevaporation grows quickly and it can finally reach ~372 au. Although external FUV photoevaporation is very weak in this case, the gravitational potential well is shallow at the large radius of the disk. The external photoevaporation can still cut off the disk and decrease R_{disk} effectively, as shown in Figure 9.

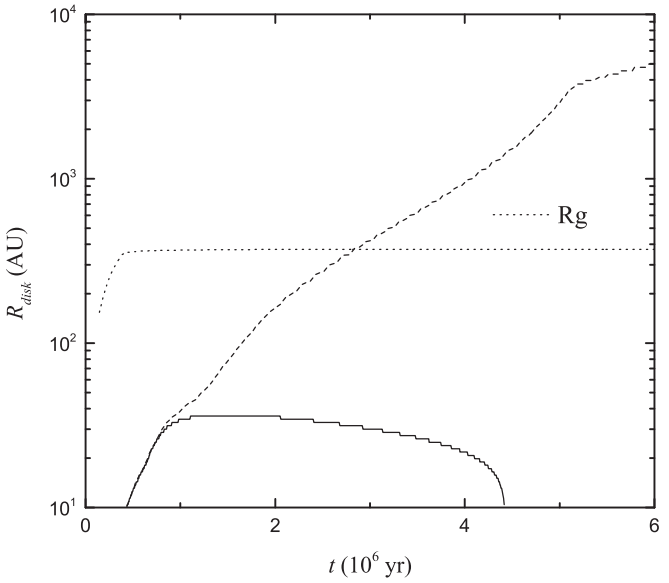

Figure 9. Evolution of R_{disk} and R_g as a function of t for the same core properties as those shown in Figures 6 and 7. The solid line represents the evolution of R_{disk} in the disk, including both internal X-ray and external FUV photoevaporations. The dashed line represents the evolution of R_{disk} in the disk, including internal X-ray photoevaporation only. The dotted line represents the evolution of R_g in the disk, including both internal X-ray and external FUV photoevaporations.

Next, we discuss the evolution of external FUV photoevaporating disks with high ω. We first present the results of the disk evolution, including internal X-ray photoevaporation only. Figure 10 shows the evolution of Σ of the internal X-ray photoevaporating disk for the high low ω case that $\omega = 5.0 \times 10^{-14}\,s^{-1}$, $T_{cd} = 10$ K, and $M_{cd} = 1.0\ M_{\odot}$. In this case, the angular momentum of the pre-stellar core is very high. Most material of the core collapses onto the disk and is far from the central star. The disk expands faster and farther compared with the case shown in Figure 1. The large R_{disk} and high Σ at the large radius of the disk make the disk dissipate slowly. Therefore, its lifetime is very long (>2×10^7 year). We then add the effect of external FUV photoevaporation in the disk with $\omega = 5.0 \times 10^{-14}\,s^{-1}$, $T_{cd} = 10$ K, and $M_{cd} = 1.0\ M_{\odot}$. The evolution of Σ is shown in Figure 11. For the high ω case, there are more materials falling onto the disk from the envelop directly rather than onto the central star during the core collapse. So, M_* is low, which means that the gravitational potential well is very shallow. In addition, M_{disk} is high and R_{disk} is large in this stage. External FUV photoevaporation is very effective during the collapse of the core. As a result, the mass supply from the collapsing cloud core cannot offset the mass loss due to accretion and photoevaporation in the early evolution of the disk. Although the disk can expand under the action of the core collapse, Σ decreases. The evolution processes described above result in the slow growth rate of the central star, which in turn further promote the external FUV photoevaporation. After the core collapse ends, the external FUV photoevaporation is so powerful that the disk shrinks and Σ decreases rapidly within $\sim 3.71 \times 10^5$ years. The disk lifetime ($\sim 1.1 \times 10^6$ years) is very short for the case with $\omega = 5.0 \times 10^{-14}\,s^{-1}$. The big difference in the disk lifetimes shown in Figures 11 and 10 indicates that the disk evolution

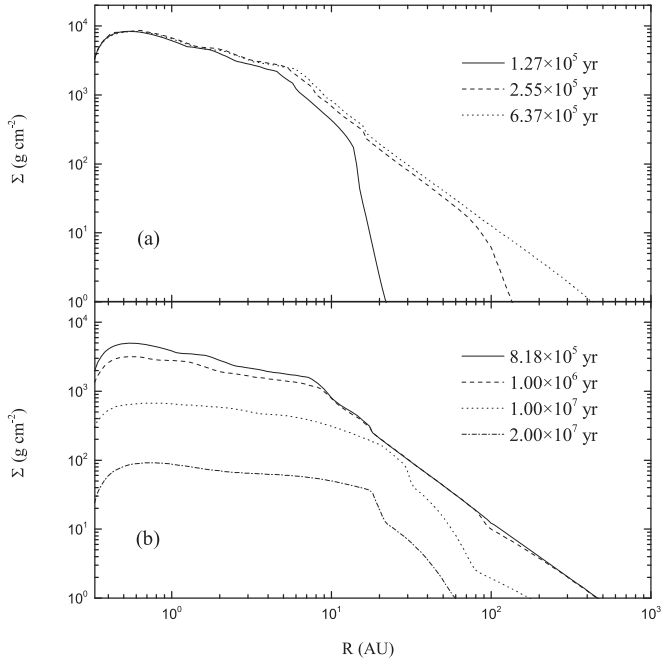

Figure 10. Evolution of Σ for the disk, including internal X-ray photoevaporation only, with $\omega = 5.0 \times 10^{-14}\,s^{-1}$, $T_{cd} = 10$ K, and $M_{cd} = 1.0\,M_\odot$. The collapse timescale of the pre-stellar core is about 6.37×10^5 years. The top panel represents the evolution of Σ before core collapse stops. The bottom panel represents the evolution of Σ after core collapse stops. The disk lifetime is longer than that shown in Figure 1. See the text for details.

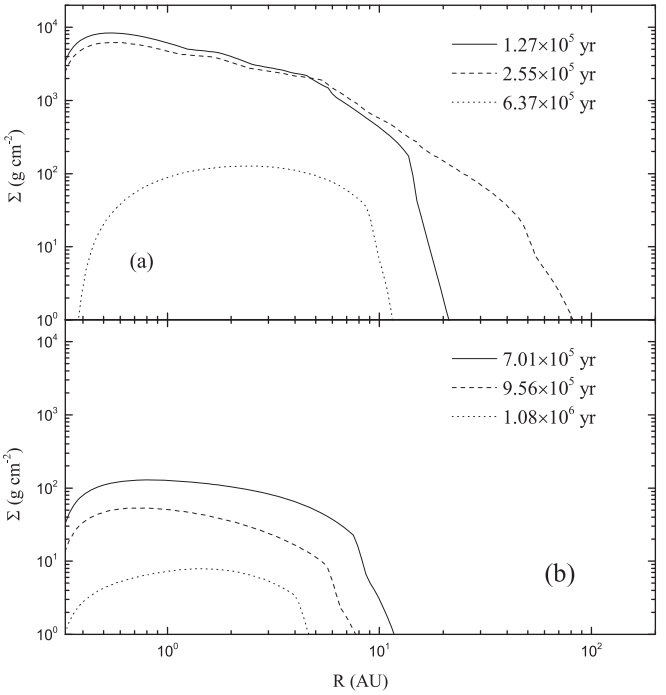

Figure 11. Evolution of Σ for the disk, including both internal X-ray and external FUV photoevaporations, with $\omega = 5.0 \times 10^{-14}\,s^{-1}$, $T_{cd} = 10$ K, $M_{cd} = 1.0\,M_\odot$, and $G_0 = 3000$ Habings. The collapse timescale of the pre-stellar core is about 6.37×10^5 years. The top panel represents the evolution of Σ before core collapse stops. The bottom panel represents the evolution of Σ after core collapse stops. The disk lifetime is much shorter than that shown in Figure 10. See the text for details.

with high ω in clusters is primarily driven by the external FUV photoevaporation.

In Figure 12, we show M_{disk} and M_* as functions of t for the disk evolutions ($\omega = 5.0 \times 10^{-14}\,s^{-1}$, $T_{cd} = 10$ K, and $M_{cd} = 1.0\,M_\odot$) with and without external FUV fields. For the disk without external FUV fields, the evolutions of M_{disk} and M_* are similar to that shown in Figure 3. Because ω is high, more material of the core falls onto the disk. When the collapse ends, M_* is about 0.34 $M_\odot$ and M_{disk} is about 0.66 $M_\odot$. After that, M_{disk} decreases and M_* increases slowly. For the disk with external FUV fields, the evolutions of M_{disk} and M_* are very different from that shown in Figure 3. The external FUV photoevaporation is very strong for the case with $\omega = 5.0 \times 10^{-14}\,s^{-1}$. Before the core collapse ends, M_{disk} has decreased. The maximum value it reached is only about 0.15 $M_\odot$. Since most material of the disk is evaporated by external FUV radiations, the final value of M_* is also low (∼0.23 $M_\odot$).

Figure 13 shows R_{disk} as a function of t for the disk evolutions $\omega = 5 \times 10^{-14}\,s^{-1}$, $T_{cd} = 10$ K, and $M_{cd} = 1.0\,M_\odot$. The high value of ω means that most material of the pre-stellar core falls onto the disk and is far from the star. So, R_{disk} for the disk without external FUV fields shown in Figure 13 is much larger than that shown in Figure 4. Since the external FUV photoevaporation is very strong, M_* is very low during the disk formation and evolution and R_g of the disk with external FUV photoevaporation is small (∼90 au), as shown in Figure 13. The strong external FUV photoevaporation also makes $R_{disk} < R_g$ with the maximum value ∼75 au. Before the core collapse ending, R_{disk} has decreased, as shown in Figure 13.

Figure 14 shows $\dot{M}_{acc}$ as a function of t with different ω for external FUV photoevaporating disks. For the low ω case

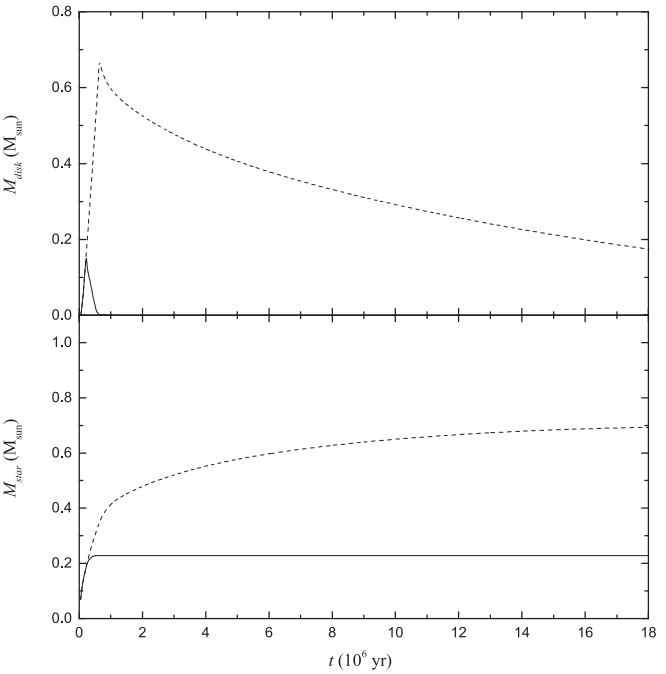

Figure 12. Evolution of M_{disk} (top panel) and M_* (bottom panel) as functions of t for the same core properties as those shown in Figures 10 and 11. The solid lines represent the case for including both internal X-ray and external FUV photoevaporations. The dashed lines represent the case for including internal X-ray photoevaporation only.

($\omega = 0.3 \times 10^{-14}\,s^{-1}$), Σ is high near the star during the core collapse shown in Figure 7. Therefore, $\dot{M}_{acc}$ is very high in the early evolution of the disk. Since R_{disk} is relatively small, the

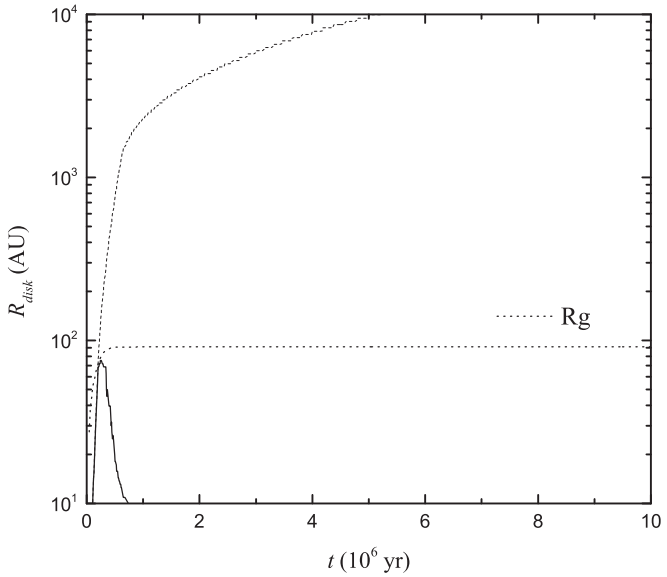

Figure 13. Evolution of $R_{\rm disk}$ and R_g as a function of t for the same core properties as those shown in Figures 10 and 11. The solid line represents the evolution of $R_{\rm disk}$ in the disk, including both internal X-ray and external FUV photoevaporations. The dashed line represents the evolution of $R_{\rm disk}$ in the disk, including internal X-ray photoevaporation only. The dotted line represents the evolution of R_g in the disk, including both internal X-ray and external FUV photoevaporations.

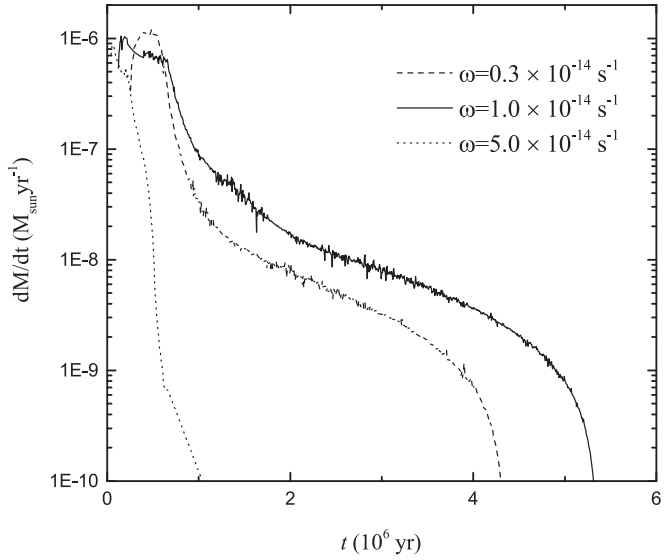

Figure 14. Evolution of $\dot{M}_{\rm acc}$ as a function of t in disks including both internal X-ray and external FUV photoevaporations with different ω. Other parameters are the same as those in Figure 2 with $T_{\rm cd} = 10$ K, $M_{\rm cd} = 1.0\ M_\odot$, and $G_0 = 3000$ Habings. The solid line represents the evolution of $\dot{M}_{\rm acc}$ in the disk with $\omega = 1.0 \times 10^{-14}\ {\rm s}^{-1}$. The dashed line represents the evolution of $\dot{M}_{\rm acc}$ in the disk with $\omega = 0.3 \times 10^{-14}\ {\rm s}^{-1}$. The dotted line represents the evolution of $\dot{M}_{\rm acc}$ in the disk with $\omega = 5.0 \times 10^{-14}\ {\rm s}^{-1}$.

viscous evolution of the disk is effective, and Σ decreases quickly. So $\dot{M}_{\rm acc}$ decreases quickly with t for the low ω case compared with the case for $\omega = 1.0 \times 10^{-14}\ {\rm s}^{-1}$. For the high ω case ($\omega = 5.0 \times 10^{-14}\ {\rm s}^{-1}$.), most materials of the core envelop fall onto the outer disk. So Σ near the star is low and $\dot{M}_{\rm acc}$ is also low. External FUV photoevaporation is strong in this case as discussed above, thus Σ decreases very quickly, which leads to $\dot{M}_{\rm acc}$ decreasing sharply.

3.3. Comparison with Other Studies

We compare our results with those in Anderson et al. (2013), who investigated the properties of disks in clusters by combining the viscous disk model with the external FUV photoevaporation model. We confirm the conclusions of Anderson et al. (2013) that external FUV photoevaporation is the dominant mechanism in truncating disk radii. We also compare our results with that in Kalyaan et al. (2015), who also include the non-uniform α in the external photoevaporating disk. Kalyaan et al. (2015) derive α from the numerical results of non-ideal magnetohydrodynamics (MHD) simulations by Bai & Stone (2011), who incorporate the effects of Ohmic resistivity and ambipolar diffusion. Although we do not consider ambipolar diffusion, we also reproduce the findings of Kalyaan et al. (2015) that non-uniform α makes a steep profile of Σ and photoevaporation steepens the slope in the outer disk (see Figure 2). Anderson et al. (2013) and Kalyaan et al. (2015) suggest that the efficiency of external FUV photoevaporation is proportional to the strength of FUV fields. The main improvement in our disk model is that we consider the process of disk formation. As discussed in Sections 3.1 and 3.2, the efficiency of external FUV photoevaporation is also the function of initial conditions of disk formation, such as ω. We find that the efficiency of external photoevaporation is very low for the low ω case ($\omega = 0.3 \times 10^{-14}\ {\rm s}^{-1}$), even if external FUV radiation is strong ($G_0 = 3000$ Habings).

4. Implications

Our calculations can interpret some observational features of disks in clusters, which may originate from the diversity of pre-stellar cores in molecular clouds. According to the *Hubble Space Telescope* (*HST*) images of ONC (Bally et al. 2000), Vicente & Alves (2005) presented the diameter distribution of disks in the Trapezium cluster. Although they did not find any disks with $R_{\rm disk} < 30$ au due to the resolution limitation, they showed that $R_{\rm disk}$ was well described as a power-law fit with an exponent of -1.9 ± 0.3. Their observations estimated that about 60% of the disks in the Trapezium had radii smaller than 50 au. Our calculations find a similar trend: for disks with different ω, the duration with $R_{\rm disk} > 50$ au is very short and for most of the time of the disk evolution, $R_{\rm disk}$ is very small (Figure 4, 9, and 13). Vicente & Alves (2005) also considered that there was no correlation between $R_{\rm disk}$ and M_*. However, we suggest that the relation between $R_{\rm disk}$ and M_* indicates the features of disk formation and evolution. For disks with small $R_{\rm disk}$ and low M_*, our model considers that they form from a per-stellar core collapse with high ω (Figure 12 and 13). The disk lifetime is very short and the star is very young. While, for disks with small $R_{\rm disk}$ and relatively high M_*, they form from a pre-stellar core collapse with low ω. The disk lifetime is long and the star is relatively old.

We then discuss the observations of $\dot{M}_{\rm acc}$ in the ONC. Manara et al. (2012) estimated $\dot{M}_{\rm acc}$ from both the U-band excess and the Hα photometry based on *HST*/WFPC2 observations. They established the relation between $\dot{M}_{\rm acc}$ and M_*, in which the factor of star age was also taken into account. Their results showed the same trend as that found in Taurus, Lupus, and Chamaeleon I (e.g., Hartmann et al. 1998; Andrews & Williams 2005; Ricci et al. 2010; Alcalá et al. 2014, 2017; Manara et al. 2014, 2016a, 2016b, 2017; Pascucci et al. 2016): $\dot{M}_{\rm acc}$ increases with M_* and decreases with evolutionary time.

They considered that there was no clear evidence for disks suffering external radiations. However, we find that for stars with $M_* \lesssim 0.2\ M_\odot$, $\dot{M}_{\rm acc}$ has a larger dispersion compared with that in Taurus (Jones et al. 2012). We suggest that the large $\dot{M}_{\rm acc}$ dispersion shown in Manara et al. (2012) results from the effects of the combination of external radiations and initial conditions for disk formation. Our numerical results show that these disks form from the pre-stellar core collapse with relatively high ω (Figure 12). As discussed in the previous section, for higher ω ($\omega = 5.0 \times 10^{-14}\ {\rm s}^{-1}$), there are more materials that fall onto the disk from the envelop directly rather than onto the central star, so the gravitational potential well is very shallow. The external FUV photoevaporation is very strong so that the disk lifetime is very short and the central star mass is very low. Therefore, $\dot{M}_{\rm acc}$ is very low ($\sim 10^{-11} M_\odot\ {\rm yr}^{-1}$) for low-mass star of young age ($<2 \times 10^6$ years). On the contrary, if we decrease ω, the external FUV photoevaporation is weakened. The disk lifetime becomes long. So, for the case of low-mass stars with similar ages, $\dot{M}_{\rm acc}$ is large ($\sim 10^{-8} M_\odot\ {\rm yr}^{-1}$) the disk with relatively low ω.

We notice that $M_{\rm disk}$ calculated in our model ($\sim$0.001–0.4 $M_\odot$) is at least 10 times higher than the observed values ($\sim$0.0001–0.01 $M_\odot$) (Mann & Williams 2010; Mann et al. 2014). This difference may derive from the uncertainty of dust observations. The mass of a disk is best determined by (sub)millimeter wavelength observations of dust (e.g., Beckwith et al. 1990; Williams & Cieza 2011), and the assumption with a gas-to-dust ratio of 100 is often adopted. This method ignores the dust growth to larger size, which can dramatically decrease the value of the dust mass opacity (D'Alessio et al. 2001). So $M_{\rm disk}$ derived from the dust observation should be considered as the lower limits. On the other hand, $M_{\rm disk}$ can also be estimated from the relation between accretion rates and protostellar ages (Hartmann et al. 1998; Andrews & Williams 2007). Mann & Williams (2010) suggest that $M_{\rm disk}$ may be underestimated by a factor of 4–8 with dust observations. Considering the uncertainty of dust observations discussed above, our calculations could fit the observed values of $M_{\rm disk}$.

5. Conclusions

In this paper, we construct a protoplanetary disk model that includes mass infall from the pre-stellar cloud core and the effect of external photoevaporation. We simulate the disk evolution to investigate the influence of core properties on the efficiency of external photoevaporation. Our calculations confirm that the external FUV photoevaporation is the dominant mechanism in truncating disk radii. The disk lifetime is shorter compared with that suffered by the internal photoevaporation only.

We show that the efficiency of external FUV photoevaporation is not only determined by the strength of FUV fields, but also determined by initial conditions of disk formation, such as ω. For the core with low ω ($\omega = 0.3 \times 10^{-14}\ {\rm s}^{-1}$), the angular momentum of the system is low. Most materials of the core collapse directly onto the central star or onto the disk near the star. The star mass is high and the initial disk size is small. The gravitational potential well of the disk is deep, so external photoevaporation is suppressed. The evolution of the disk is primarily driven by its own internal viscosity. Since the disk mass is relatively low, the disk lifetime is short. As ω increases to $\sim 1.0 \times 10^{-14}\ {\rm s}^{-1}$, more materials of the core fall onto the disk. Although external photoevaporation is enhanced, it still cannot offset the mass supply from the collapsing core and suppress the disk expansion in the early evolution of the system. Therefore, the disk size is large and the disk mass is high, which lead to the long disk lifetime. The final mass of the star decreases compared with the case $\omega = 0.3 \times 10^{-14}\ {\rm s}^{-1}$ due to the high external photoevaporation rate. If ω is high enough ($\omega = 5.0 \times 10^{-14}\ {\rm s}^{-1}$), most materials of the core fall onto the disk far from the central star. The star mass is so low that the gravitational potential well of the disk is very shallow. The effects of external FUV photoevaporation are very strong. Most of materials in the disk are evaporated. As a result, the disk lifetime is very short and the final mass of the central star is very small. Our calculations reveal that even if the external FUV radiation is strong, the efficiency of external photoevaporation is still very low when ω is low (such as $\omega = 0.3 \times 10^{-14}\ {\rm s}^{-1}$). Previous studies on external photoevaporation in disks do not consider how a disk forms, so the effects of initial conditions of disk formation on the disk evolution in clusters are ignored (e.g., Adams et al. 2004; Anderson et al. 2013; Kalyaan et al. 2015).

Our calculations can interpret some observational features of disks in clusters. We confirm the observed estimation that most disks in the clusters have radii smaller than 50 au. We suggest that the correlation between $R_{\rm disk}$ and M_* reveals the initial conditions of the formation of protostar+disk systems. The disks with small $R_{\rm disk}$ and low M_* form from a pre-stellar core collapse with high ω. While the disks with small $R_{\rm disk}$ and high M_*, form from a pre-stellar core collapse with low ω. We also suggest that the large dispersion of $\dot{M}_{\rm acc}$ for low-mass stars ($M_* \lesssim 0.2\ M_\odot$) is the result of the diversity of ω. Our calculation results of $M_{\rm disk}$ are consistent with the estimation from the relation between accretion rates and protostellar ages. We suggest that the disk mass determined by (sub)millimeter wavelength observations of dust may be underestimated.

We are grateful to the anonymous referee for constructive and fruitful comments that helped us improve our paper significantly. This research is supported by the National Natural Science Foundation of China (NSFC) grant No. 11703075, West Light Foundation of CAS (2017-QNXZ-B), and Xinjiang Tianchi Bairen project. L.X. thanks the Key Laboratory for the Structure and Evolution of Celestial Objects of CAS for foundation support (grant No. OP201711). Q.C. is a research fellow of the One Hundred Talents project of the Chinese Academy of Sciences. He also acknowledges support from the National Natural Science Foundation of China (NSFC) grant No. 11673054.

ORCID iDs

Lin Xiao https://orcid.org/0000-0002-9511-7062
Qiang Chang https://orcid.org/0000-0002-0040-6022

References

Adams, F. C., Hollenbach, D., Laughlin, G., & Gorti, U. 2004, ApJ, 611, 360
Alcalá, J. M., Manara, C. F., Natta, A., et al. 2017, A&A, 600, A20
Alcalá, J. M., Natta, A., Manara, C. F., et al. 2014, A&A, 561, A2
Anderson, K. R., Adams, F. C., & Calvet, N. 2013, ApJ, 774, 9
Andrews, S. M., & Williams, J. P. 2005, ApJ, 631, 1134
Andrews, S. M., & Williams, J. P. 2007, ApJ, 671, 1800
Andrews, S. M., Wilner, D. J., Hughes, A. M., Qi, C., & Dullemond, C. P. 2009, ApJ, 700, 1502
Ansdell, M., Williams, J. P., Manara, C. F., et al. 2017, AJ, 153, 240
Ansdell, M., Williams, J. P., van der Marel, N., et al. 2016, ApJ, 828, 46

Armitage, P. J. 2011, ARA&A, 49, 195
Armitage, P. J., Clarke, C. J., & Palla, F. 2003, MNRAS, 342, 1139
Bae, J., Hartmann, L., Zhu, Z., & Gammie, C. 2013, ApJ, 774, 57
Bai, X.-N. 2014, ApJ, 791, 137
Bai, X.-N., & Stone, J. M. 2011, ApJ, 736, 144
Balbus, S. A., & Hawley, J. F. 1991, ApJ, 376, 214
Balbus, S. A., & Hawley, J. F. 1998, RvMP, 70, 1
Bally, J., O'Dell, C. R., & McCaughrean, M. J. 2000, AJ, 119, 2919
Bally, J., Testi, L., Sargent, A., & Carlstrom, J. 1998, AJ, 116, 854
Bath, G. T., & Pringle, J. E. 1981, MNRAS, 194, 967
Beckwith, S. V. W., Sargent, A. I., Chini, R. S., & Guesten, R. 1990, AJ, 99, 924
Bell, K. R., Cassen, P. M., Klahr, H. H., & Henning, T. 1997, ApJ, 486, 372
Bonnell, I. A., Bate, M. R., & Vine, S. G. 2003, MNRAS, 343, 413
Bonnor, W. B. 1956, MNRAS, 116, 351
Boss, A. P. 1993, ApJ, 410, 157
Carpenter, J. M. 2002, AJ, 124, 1593
Caselli, P., Benson, P. J., Myers, P. C., & Tafalla, M. 2002, ApJ, 572, 238
Cassen, P. 1994, Icar, 112, 405
Cassen, P., & Moosman, A. 1981, Icar, 48, 353
Chambers, J. E. 2006, ApJL, 652, L133
Champion, J., Berné, O., Vicente, S., et al. 2017, A&A, 604, A69
Churchwell, E., Felli, M., Wood, D. O. S., & Massi, M. 1987, ApJ, 321, 516
Ciesla, F. J., & Cuzzi, J. N. 2006, Icar, 181, 178
Cieza, L., Williams, J., Kourkchi, E., et al. 2015, MNRAS, 454, 1909
Clarke, C. J. 2007, MNRAS, 376, 1350
Clarke, C. J., Gendrin, A., & Sotomayor, M. 2001, MNRAS, 328, 485
Da Rio, N., Robberto, M., Soderblom, D. R., et al. 2009, ApJS, 183, 261
D'Alessio, P., Calvet, N., & Hartmann, L. 2001, ApJ, 553, 321
DeSouza, A. L., & Basu, S. 2017, NewA, 51, 113
Dubrulle, B. 1993, Icar, 106, 59
Ebert, R. 1955, ZA, 37, 217
Eisner, J. A., Bally, J. M., Ginsburg, A., & Sheehan, P. D. 2016, ApJ, 826, 16
Eisner, J. A., & Carpenter, J. M. 2003, ApJ, 598, 1341
Eisner, J. A., & Carpenter, J. M. 2006, ApJ, 641, 1162
Eisner, J. A., Plambeck, R. L., Carpenter, J. M., et al. 2008, ApJ, 683, 304
Ercolano, B., Clarke, C. J., & Drake, J. J. 2009, ApJ, 699, 1639
Facchini, S., Clarke, C. J., & Bisbas, T. G. 2016, MNRAS, 457, 3593
Fleming, T., & Stone, J. M. 2003, ApJ, 585, 908
Gammie, C. F. 1996, ApJ, 457, 355
Goodman, A. A., Benson, P. J., Fuller, G. A., & Myers, P. C. 1993, ApJ, 406, 528
Gressel, O., Turner, N. J., Nelson, R. P., & McNally, C. P. 2015, ApJ, 801, 84
Habing, H. J. 1968, BAN, 19, 421
Hartmann, L., Calvet, N., Gullbring, E., & D'Alessio, P. 1998, ApJ, 495, 385
Hatchell, J., Wilson, T., Drabek, E., et al. 2013, MNRAS, 429, L10
Haworth, T. J., Boubert, D., Facchini, S., Bisbas, T. G., & Clarke, C. J. 2016, MNRAS, 463, 3616
Hennebelle, P., Whitworth, A. P., Cha, S.-H., & Goodwin, S. P. 2004, MNRAS, 348, 687
Henney, W. J., & O'Dell, C. R. 1999, AJ, 118, 2350
Howard, A. W. 2013, Sci, 340, 572
Hubickyj, O., Bodenheimer, P., & Lissauer, J. J. 2005, Icar, 179, 415
Hueso, R., & Guillot, T. 2005, A&A, 442, 703
Jijina, J., Myers, P. C., & Adams, F. C. 1999, ApJS, 125, 161
Jin, L. 1996, ApJ, 457, 798
Jin, L., & Sui, N. 2010, ApJ, 710, 1179
Johnstone, D., Hollenbach, D., & Bally, J. 1998, ApJ, 499, 758
Jones, M. G., Pringle, J. E., & Alexander, R. D. 2012, MNRAS, 419, 925
Kalyaan, A., Desch, S. J., & Monga, N. 2015, ApJ, 815, 112
Kim, J. S., Clarke, C. J., Fang, M., & Facchini, S. 2016, ApJL, 826, L15
Klahr, H. H., & Bodenheimer, P. 2003, ApJ, 582, 869
Kratter, K., & Lodato, G. 2016, ARA&A, 54, 271
Kratter, K. M., Matzner, C. D., & Krumholz, M. R. 2008, ApJ, 681, 375
Kratter, K. M., Matzner, C. D., Krumholz, M. R., & Klein, R. I. 2010, ApJ, 708, 1585
Lada, C. J., & Lada, E. A. 2003, ARA&A, 41, 57
Laughlin, G., & Bodenheimer, P. 1994, ApJ, 436, 335
Laughlin, G., Korchagin, V., & Adams, F. C. 1997, ApJ, 477, 410
Laughlin, G., Korchagin, V., & Adams, F. C. 1998, ApJ, 504, 945
Laughlin, G., & Rozyczka, M. 1996, ApJ, 456, 279
Lesur, G., Kunz, M. W., & Fromang, S. 2014, A&A, 566, A56
Li, M., & Xiao, L. 2016, ApJ, 820, 36
Lynden-Bell, D., & Pringle, J. E. 1974, MNRAS, 168, 603
Machida, M. N., Inutsuka, S.-I., & Matsumoto, T. 2010, ApJ, 724, 1006
Manara, C. F., Fedele, D., Herczeg, G. J., & Teixeira, P. S. 2016a, A&A, 585, A136
Manara, C. F., Robberto, M., Da Rio, N., et al. 2012, ApJ, 755, 154
Manara, C. F., Rosotti, G., Testi, L., et al. 2016b, A&A, 591, L3
Manara, C. F., Testi, L., Herczeg, G. J., et al. 2017, A&A, 604, A127
Manara, C. F., Testi, L., Natta, A., et al. 2014, A&A, 568, A18
Mann, R. K., Andrews, S. M., Eisner, J. A., et al. 2015, ApJ, 802, 77
Mann, R. K., Di Francesco, J., Johnstone, D., et al. 2014, ApJ, 784, 82
Mann, R. K., & Williams, J. P. 2010, ApJ, 725, 430
McKee, C. F., & Ostriker, E. C. 2007, ARA&A, 45, 565
Mills, S. M., & Mazeh, T. 2017, ApJL, 839, L8
Miotello, A., van Dishoeck, E. F., Williams, J. P., et al. 2017, A&A, 599, A113
Mitchell, T. R., & Stewart, G. R. 2010, ApJ, 722, 1115
Mulders, G. D., Pascucci, I., Manara, C. F., et al. 2017, ApJ, 847, 31
Mundy, L. G., Looney, L. W., & Lada, E. A. 1995, ApJL, 452, L137
Nakamoto, T., & Nakagawa, Y. 1994, ApJ, 421, 640
Ndugu, N., Bitsch, B., & Jurua, E. 2017, arXiv:1710.10863
O'dell, C. R., Wen, Z., & Hu, X. 1993, ApJ, 410, 696
Owen, J. E., Clarke, C. J., & Ercolano, B. 2012, MNRAS, 422, 1880
Owen, J. E., Ercolano, B., & Clarke, C. J. 2011, MNRAS, 412, 13
Owen, J. E., Ercolano, B., Clarke, C. J., & Alexander, R. D. 2010, MNRAS, 401, 1415
Pascucci, I., Testi, L., Herczeg, G. J., et al. 2016, ApJ, 831, 125
Pollack, J. B., Hubickyj, O., Bodenheimer, P., et al. 1996, Icar, 124, 62
Pringle, J. E. 1981, ARA&A, 19, 137
Rafikov, R. R. 2015, ApJ, 804, 62
Rafikov, R. R. 2017, ApJ, 837, 163
Reggiani, M., Robberto, M., Da Rio, N., et al. 2011, A&A, 534, A83
Ricci, L., Testi, L., Natta, A., et al. 2010, A&A, 512, A15
Rosotti, G. P., Clarke, C. J., Manara, C. F., & Facchini, S. 2017, MNRAS, 468, 1631
Ruden, S. P., & Lin, D. N. C. 1986, ApJ, 308, 883
Shakura, N. I., & Sunyaev, R. A. 1973, A&A, 24, 337
Shu, F. H. 1977, ApJ, 214, 488
Shu, F. H., Adams, F. C., & Lizano, S. 1987, ARA&A, 25, 23
Toomre, A. 1964, ApJ, 139, 1217
Udry, S., & Santos, N. C. 2007, ARA&A, 45, 397
Umebayashi, T. 1983, PThPh, 69, 480
Vicente, S. M., & Alves, J. 2005, A&A, 441, 195
Vorobyov, E. I. 2010, ApJ, 723, 1294
Vorobyov, E. I., & Basu, S. 2006, ApJ, 650, 956
Williams, J. 2010, ConPh, 51, 381
Williams, J. P., Andrews, S. M., & Wilner, D. J. 2005, ApJ, 634, 495
Williams, J. P., & Cieza, L. A. 2011, ARA&A, 49, 67
Xiao, L., Jin, L., Liu, C., & Fan, C. 2016, ApJ, 826, 168
Xiao, L., Niu, R., & Zhang, H. 2017, MNRAS, 467, 2869
Xie, J.-W., Dong, S., Zhu, Z., et al. 2016, PNAS, 113, 11431
Zhu, Z., Hartmann, L., & Gammie, C. 2010, ApJ, 713, 1143
Zhu, Z., Hartmann, L., Nelson, R. P., & Gammie, C. F. 2012, ApJ, 746 110